Available online at www.sciencedirect.com
ScienceDirect
International Journal of Multiphase Flow 33 (2007) 164–181
International Journal of Multiphase Flow
www.elsevier.com/locate/ijmulflow

Dynamical features of the solid motion in gas–solid risers

Satish Bhusarapu [a,1], Miryan Cassanello [b,*], Muthanna H. Al-Dahhan [a], Milorad P. Dudukovic [a], Steven Trujillo [c], Timothy J. O'Hern [c]

[a] *Chemical Reaction Engineering Laboratory, Department of Chemical Engineering, Campus Box 1198, 1 Brookings Drive, Washington University, St. Louis, MO 63130-4899, USA*
[b] *PINMATE, Departamento de Industrias, Facultad de Ciencias Exactas y Naturales, Universidad de Buenos Aires, Ciudad Universitaria, Int. Güiraldes 2620, Buenos Aires C1428BGA, Argentina*
[c] *Sandia National Laboratories, Engineering Sciences Center, MS 0834, P.O. Box 5800, Albuquerque, NM 87185, USA*

Received 7 April 2006; received in revised form 9 August 2006

Abstract

The trajectories of a solid tracer with the same characteristics as the circulating solids in the risers of two pilot-scale circulating fluidized beds (CFBs), obtained by the computer automated radioactive particle tracking (CARPT) technique, are examined in detail to get further insights into the complex solids dynamics of these systems. The analysis uses tools from the theory of non-linear dynamics and symbolic dynamics. Distinct features of the solids dynamics within the fast fluidization and the dilute phase transport flow regimes are highlighted and related to the operating conditions. The possibility of downflow cluster existence within the central region of the riser is particularly examined.

Keywords: Gas–solid risers; Circulating fluidized beds; Solids dynamics; CARPT

1. Introduction

Circulating fluidized beds (CFB) are extensively used for several chemical processes involving gas–solid reactions, mainly in the petroleum and petrochemical industries and in mineral processing. A thorough conception of the particle motion in the risers of CFBs is highly desirable to develop fundamental models for proper design and scale-up of these units. Moreover, existing and new models aimed at describing the complex particle dynamics in CFBs require experimental data for validation and improvement (Berruti et al., 1995; Sinclair, 2000; Huilin et al., 2005).

We have recently reported information of the overall solids motion and distribution and some characteristics of the solids flow mixing within a section of the riser of two pilot-scale circulating fluidized beds (CFBs), obtained by the computed automated radioactive particle tracking (CARPT) technique and by gamma ray

* Corresponding author. Tel.: +54 11 4576 3383; fax: +54 11 4576 3366.
E-mail address: miryan@di.fcen.uba.ar (M. Cassanello).
[1] Present address: Harper International Corporation, 100 West Drullard Avenue, Lancaster, NY 14086, USA.

0301-9322/$ - see front matter
doi:10.1016/j.ijmultiphaseflow.2006.08.006

computed tomography (Bhusarapu et al., 2005, 2006). The great advantage of these techniques is their capability of non-intrusively exploring the 3D structure and the complex solids motion in large opaque systems. A comprehensive literature survey of the available experimental information of solids flow and mixing in CFBs has been presented and discussed in Bhusarapu et al. (2006). Most of the available information either relies on invasive methodologies or are restricted to laboratory systems, 2D configurations, or have some particular design, which prevents recovering the actual path of a particle with exactly the same characteristics as the flowing solids.

From the analysis of CARPT data reported in Bhusarapu et al. (2005), features of the solids motion were highlighted and related to the operating conditions. To get further insights into the complex solids flow patterns, in this contribution, the trajectories of the radioactive tracer in the risers of pilot-scale CFBs are analyzed with tools borrowed from the theory of non-linear dynamics and of symbolic dynamics. The solids motion under two different flow regimes, fast fluidization (FF) and dilute phase transport (DPT), is examined. A data-mining approach is also applied to recover some features of the solids actual motion from the long tracing periods of observation. Hypothesis concerning the flow regime characteristics put forward in our previous contributions are being explored more deeply in this work.

2. Experimental

The tracer trajectories were obtained by CARPT, performed in a section of two pilot-scale gas–solid risers. One riser, made of Pyrex glass, located in the Chemical Reaction Engineering Laboratory (CREL), has 6 in. I.D. (0.152 m) and 26 ft (7.93 m) height, with a downcomer of 2 in. I.D. (0.051 m). Data with solids mass fluxes below 40 kg m^{-2} s^{-1} were obtained in this system. The testing section, made of clear PVC, spans the region between 5 and 5.7 m. Trajectories confined to the zone going from 5.1 m ($Z/D = 33.5$) to 5.6 m ($Z/D = 36.7$), where the resolution is better, are considered for the analysis.

Experiments with high solid fluxes ($G_s > 100$ kg m^{-2} s^{-1}) were performed in the second riser that is part of a CFB at the Sandia National Laboratory (SNL). The riser, made of acrylic, has an I.D. of 0.14 m and a total height of 5.77 m. The total zone of investigation for CARPT is between 2.08 and 2.79 m, and the trajectories between 2.28 m ($Z/D = 16.3$) and 2.70 m ($Z/D = 19.3$) are analyzed.

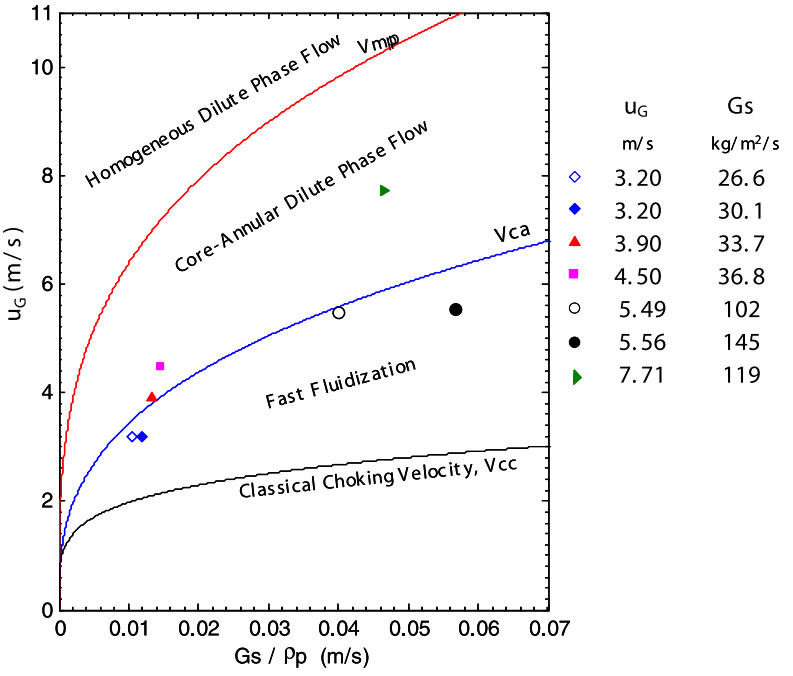

Fig. 1. Flow regime of the examined experimental conditions. Correlations for V_{cc}, V_{CA}, V_{mp} were obtained from Bi and Grace (1995).

Glass beads ($\rho_p = 2550$ kg m^{-3}) with Sauter mean diameter of 150 μm (with a standard deviation of 15 μm) were employed in the experiments. The tracer is a ^{46}Sc radionuclide particle, coated to match the density and mean diameter of the employed glass beads. Twenty detectors are located surrounding the testing section, to reconstruct the tracer instantaneous positions with a frequency of 200 Hz. Air was used as the fluidizing gas in both CFBs. Further details of the experimental installations and of the CARPT system are described in Bhusarapu (2005).

Operating conditions that lead to the fast fluidization (FF) and the dilute phase transport (DPT) flow regimes, according to the maps of Bi and Grace (1995), are examined (Fig. 1). In this flow regime map, curves for the classical choking velocity (V_{cc}), the type A choking velocity (V_{CA}) and the minimum pressure drop point (V_{mp}) were obtained from the correlations provided in Bi and Grace (1995). To determine the flow regime, operating parameters such as solids mass flux and superficial gas velocity are required. The mass flux is obtained inspecting a section where the solids are under plug flow condition. The measurements used for estimating the solids mass flux consist of: (i) tracking a single radioactive tracer particle with two NaI (Tl) scintillation detectors, to estimate the solids velocity, and (ii) measuring the solids holdup in the same section by γ-ray line densitometry. The downcomer section (2 in. column) of the CFB loop was used, since it was observed during operation that this section was always filled with a bed of solids moving in a state close to a packed bed. A complete description of the technique, and results, can be found in Bhusarapu et al. (2004).

3. Results and discussion

With CARPT, instantaneous positions of the tracer are determined every 5 ms during extended periods of observation. The ability of CARPT to reconstruct the actual path of the particle has already been discussed in Bhusarapu et al. (2005, 2006). Trajectories of the solid tracer in the inspected gas–solid risers are generally composed by fast ascending motions traversing rapidly the whole testing section, superimposed to recirculation paths and periods of stagnancy or slowly descending circulation of the tracer, mainly near the wall (Bhusarapu et al., 2005, 2006). Solids residence time distributions and solids mixing features have been found to be markedly different in the FF and DPT flow regimes.

3.1. Non-linear dynamics theory

Non-linear dynamics theory has provided a framework and a new set of tools suitable for analysis of experimental time series, which frequently contributes to get further insights in the dynamics of complex systems (Schreiber, 1999). It is particularly appropriate for systems with chaotic characteristics. However, as discussed by Takens (2003), even for stochastic systems, the tools developed within the theory of non-linear dynamics, based on computing correlation integrals, can be used to distinguish between different dynamical regimes.

The analysis from the viewpoint of the theory of non-linear dynamics has proved to be successful in aiding the understanding of fluidized bed dynamics from inspection of characteristic variables time series (see for instance Daw et al., 1990; van den Bleek et al., 2002; Bai et al., 1999; Ji et al., 2000; Huilin et al., 2002; Wu et al., 2006, and references therein). Moreover, it has contributed to establish a detailed classification of flow regimes and identification of flow regime transitions from pressure fluctuation time series acquired in CFBs of different sizes (Zijerveld et al., 1998; Johnsson et al., 2000). It has also allowed inferring features of the solids motion in three-phase fluidized beds from the analysis of a solid tracer path obtained by radioactive particle tracking (Cassanello et al., 1995). In this context, it becomes interesting to examine the actual motion of one of the solid particles immersed in the flow of pilot-scale CFBs using some of these tools.

By computing the time intervals between successive crossings of the tracer at a given height within the riser, and also with a given direction, first-return maps have been obtained from the axial coordinate of the radioactive particle. The considered height for computing the cross was the middle of the test section, where the position resolution is good. Also, only crossings separated by at least five sampling periods are taken into account to reduce the influence of noise. The angular descriptions of the obtained maps in polar coordinates are illustrated in Fig. 2, for different gas velocities and solids mass fluxes.

For experiments in the fast fluidization (FF) regime, the points are uniformly distributed, which suggests an almost random motion of the particle. In contrast, in the core-annular dilute phase flow (dilute phase

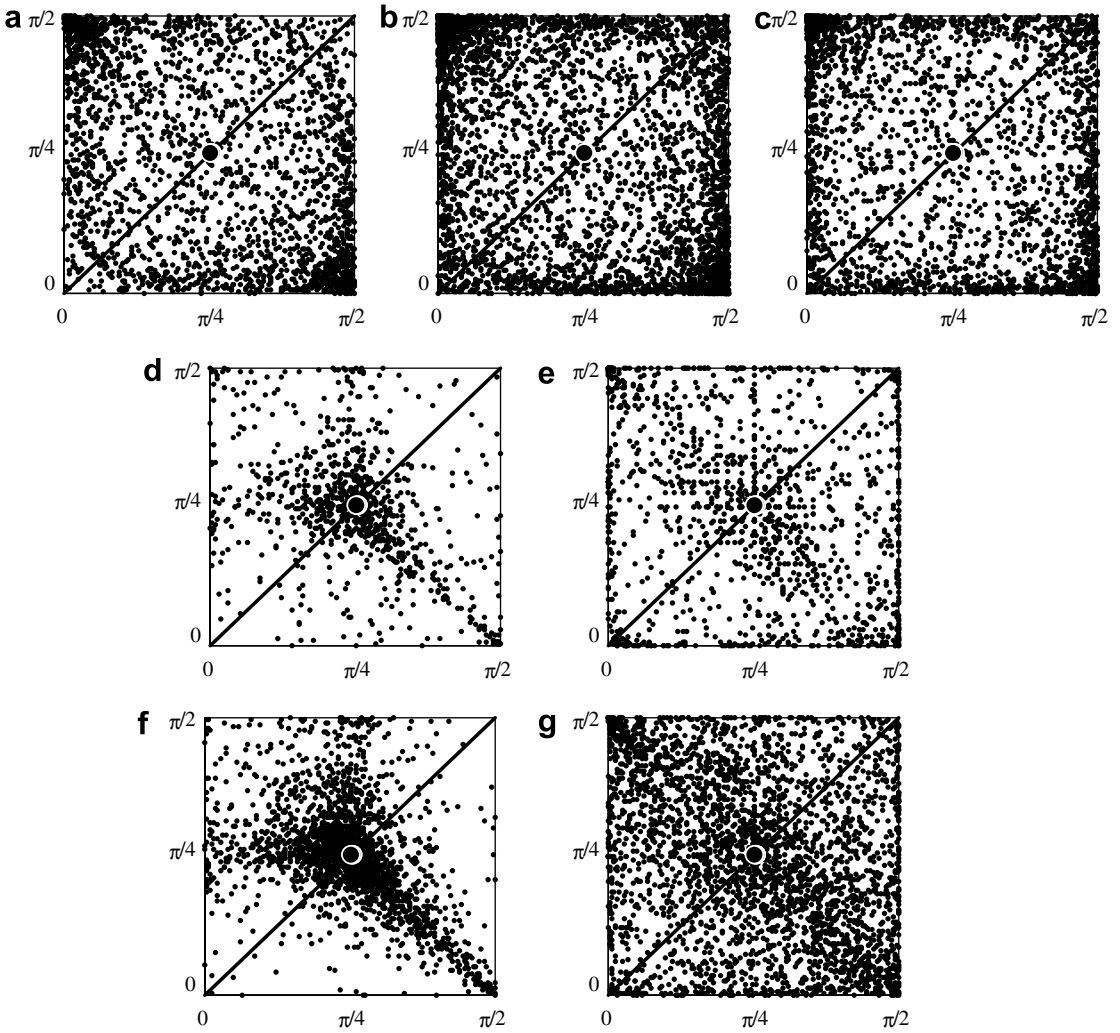

Fig. 2. Angular return maps (φ_{i+1} vs φ_i), calculated from successive crosses of the radioactive tracer through a given height in the riser, for different gas velocities, u_G, and solid mass flux, G_s. Expanded flow regimes: (a–c) fast fluidization and (d–g) core-annular diluted phase flow. (a) $u_G = 3.20$ m/s, $G_s = 26.6$ kg/m^2 s; (b) $u_G = 3.20$ m/s, $G_s = 30.1$ kg/m^2 s; (c) $u_G = 5.56$ m/s, G_s=145.0 kg/m^2 s; (d) $u_G = 3.90$ m/s, $G_s = 33.7$ kg/m^2 s; (e) $u_G = 5.49$ m/s, $G_s = 102.0$ kg/m^2 s; (f) $u_G = 4.5$ m/s, $G_s = 36.8$ kg/m^2 s and (g) $u_G = 7.71$ m/s, $G_s = 119.0$ kg/m^2 s.

transport flow – DPT), the motion becomes more deterministic. This is reflected in the maps in spite of the degree of noise, which tends to hide the trends for some conditions, particularly at high solid fluxes (Fig. 2g). The states of the system give a more definite pattern in the DPT regime, indicating that the motion becomes more regular. The points of the angular first-return map are mostly confined close to a region on the first bisecting line, and delineate a distinguishable structure, as in the case of a purely periodic flow. Although, many states go far from the bisecting line, which suggests the presence of an intermittent mechanism on the phase angle, involving a deterministic periodicity alternating with periods of irregular dynamics. Experiments close to the flow regime boundary according to the estimated map (Fig. 1) have dynamical characteristics more similar to those in the DPT regime than in the FF regime (Fig. 2d–e).

The configuration of the angular first-return map is still recognizable in all the experiments corresponding to the core-annular dilute phase flow, even though some points spread out from the estimated curve. This means that the dynamics is mainly governed by phase intermittency and it is thus deterministic. In contrast, in the fast fluidization regime, the points of the first-return map do not seem to be confined on any structure and tend to visit all the possible positions. Consequently, the dynamics could be associated with a more

stochastic process, since no structure is easily extracted. This result highlights the great differences between the two examined flow regimes in a CFB.

To get a numerical index from the map to quantitatively characterize the differences between both dynamical regimes, the local mean information loss rate (ILR) was computed from the divergence of very close trajectories in the angular maps, starting from positions in the surroundings of the bisecting line center (shown as a black dot in the figures). The index has been calculated with the methodology used to estimate Lyapunov exponents from maps (see for instance Hilborn, 2000 or Sprott, 2003). The higher are the indexes, the faster is the divergence of close trajectories. Estimated values of the ILR index are listed in Table 1. For the FF regime, they almost double those corresponding to the DPT regime, indicating that the divergence is faster. However, values are not extremely large, pointing to a process that is not totally stochastic.

Examples of typical time series obtained by computing the time intervals between successive crossings of the test section at the mid-height ($Z/D = 35.1$ in CREL riser and $Z/D = 17.8$ in SNL riser) are illustrated in Fig. 3. In all the experiments, relatively short time lags between crossings alternate with occasionally prolonged lags. This behavior is slightly more apparent for experiments in the DPT flow regime or near the transition (Fig. 3b and d). For experiments with high solids flux, a bottom bed exists in the CFB setup at SNL, and the test section is located lower in the riser but still above the bottom bed. However, the exploding characteristics of the bubbles in the dense bottom do not seem to be the reason for the swinging between irregular and almost periodic behaviors in the time series of the DPT experiment at high solid flux (Fig. 3d), since it should be the same or even stronger for the experiment with the longer bottom bed (Fig. 3c). Considering the time elapsed between successive crossings, the alternating behavior seems to arise from local recirculation (intervals lower than 0.10 s) superimposed to longer intervals appearing with a more irregular structure.

The dynamical characteristics of the time series of intervals are also estimated by directly applying the procedures proposed by Grassberger and Procaccia (1983a,b) to calculate the Kolmogoroff entropy and the correlation dimension; results are listed in Table 1. The correlation dimension provides an indication of the active degrees of freedom of the underlying solid dynamics, while the Kolmogoroff entropy allows diagnosing whether the system is behaving as a chaotic one. In principle, physical limits exist for the Kolmogoroff entropy (KE): for a dissipative deterministic non-chaotic system, $KE = 0$; for a stochastic system, KE tends to infinite; for a deterministic chaotic system, KE is finite and positive and it is higher when the divergence of trajectories is faster (Hilborn, 2000).

As judged from Table 1, the attractors reconstructed from the time series of a solid particle in the CFBs have low dimensions. Previous works reported in the literature, which have estimated the correlation dimension from time series of other variables in CFBs, have also found low dimensions, generally below 2 (Huilin et al., 1997; Bai et al., 1996). However, the calculated dimensions are not totally independent of the variable used for the analysis, mainly due to the spatiotemporal dependence of the motion. For instance, Ji et al. (2000) found values significantly different depending on the variable used for the estimation; the authors relate this result to the ability of each variable to observe a different scale of the motion. In this case, for experiments in the DPT regime, the correlation integrals show two distinct slopes. The one that arises from closer points within the attractors, which was generally broader, was used to estimate the correlation dimensions, ν, and

Table 1
Influence of the flow regime on characteristic parameters, an index of information loss rate (ILR), the correlation dimension, ν and the Kolmogoroff entropy, KE, estimated from the tracer trajectories with tools borrowed from the theory of non-linear dynamics

Riser	u_G (m/s)	G_s (kg/m^2 s)	Flow regime	ILR index[a]	ν[b]	KE[b] (bits/s)
CREL	3.20	26.6	FF	0.89	0.81	2.05
CREL	3.20	30.1	FF	0.95	1.62	4.29
SNL	5.56	145.0	FF	0.84	0.58	1.72
CREL	3.90	33.7	Trans/DPT	0.46	0.004	0.02
SNL	5.49	102.0	Trans/DPT	0.55	0.012	0.12
CREL	4.50	36.8	DPT	0.45	0.011	0.03
SNL	7.71	119.0	DPT	0.52	0.024	0.17

[a] Calculated with procedures used to estimate Lyapunov exponents from maps (Sprott, 2003).
[b] Estimated using the methodology proposed by Grassberger and Procaccia (1983a,b).

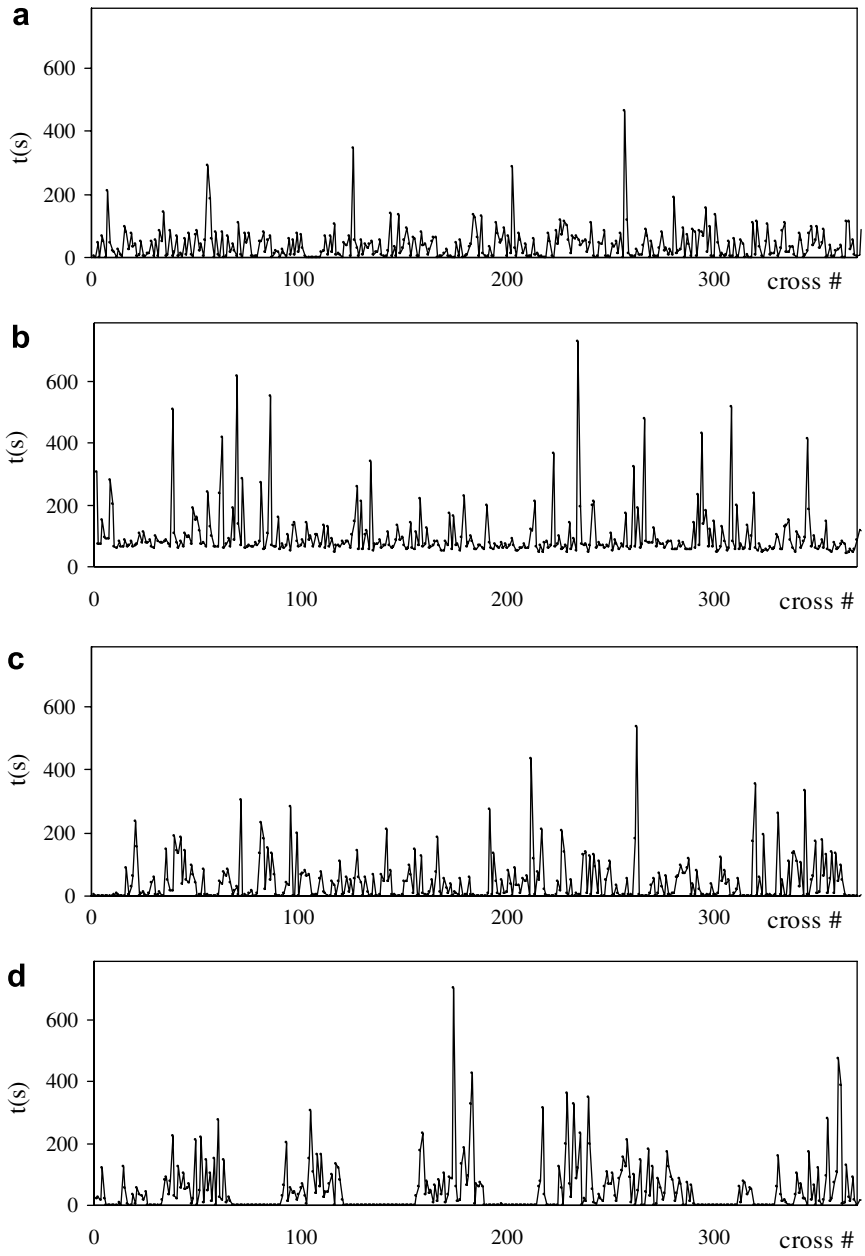

Fig. 3. Time series of intervals between successive crossings of the tracer through a given height in the riser located in the middle of the testing section for (a) $u_G = 3.2$ m/s, $G_s = 26.6$ kg/m^2 s; (b) $u_G = 4.5$ m/s, $G_s = 36.8$ kg/m^2 s; (c) $u_G = 5.56$ m/s, $G_s = 145$ kg/m^2 s and (d) $u_G = 5.49$ m/s, $G_s = 102$ kg/m^2 s.

the Kolmogoroff entropies, KE. For experiments in the FF regime, the two slopes converge. The appearance of two distinct slopes has already been found in previous works that examined the underlying dynamics of gas–solid fluidized beds from the analysis of different characteristic variables, like pressure and temperature fluctuations and local solid holdups. It was argued that it arises from the different scales covering particle fluctuations (small scale) and the time variation of voids and clusters (large scale) (Bai et al., 1999; Ji et al., 2000; Huilin et al., 2002; Wu et al., 2006).

Calculated v and KE in the DPT regime tend to values close to zero, pointing again to a dynamics of the solids motion that is more regular than in the FF regime. Experiments in the last are characterized by larger

dimensions and higher, though finite, values of KE, evidencing its chaotic nature. Even if it is difficult to compare absolute values of the KE calculated from the analysis of different variables, due to the multiscale behavior and the different algorithms used, variations in trends are generally more meaningful and consistent among results of different authors. For instance, a significant decrease in the KE estimated from pressure fluctuation time series in CFBs was also observed for the dilute phase transport flow by Zijerveld et al. (1998).

Comparing experiments with similar gas velocities, it comes out that the solids mass flux apparently exerts a significant positive influence on the Komogoroff entropy, particularly when it leads to a change in the flow regime. Zijerveld et al. (1998) also found a positive influence of the solids flux on the estimated value of the KE for circulating conditions (intermediate dilute and dilute transport flow, according to their classification) when there is no dense bottom bed. In this work, the examined solids circulation was carried out within a section of the riser where the flow is considered to be developed, far from the bottom bed. Hence, the influence of the bubbles and slugs that could exist in the bottom bed is less reflected. According to the results reported by Zijerveld et al. (1998), when a dense bottom bed is present, the exploding characteristics of the bed has an influence on KE that depends on the length of the bed. A longer bed allows a longer path for gas bubbles and slugs, inducing a periodicity reflected in more regular pressure fluctuations. The ordering in the structure arising from the existence of a dense bottom bed is clearly appreciated from experiments in a 2D CFB by particle tracking using fluorescent particles (Pallarès and Johnsson, 2006). In the experiments reported in this work, even though a bottom bed exists in the setup at SNL, the location of the test section is at a considerably higher level and apparently does not reflect the dynamics of the region proximate to the dense bed. In addition, it is likely that pressure fluctuations may be more affected by the exploding character of the bottom bed than the motion of single particles, when this motion is far above. Ji et al. (2000) found an influence of the solid mass flux on their estimated KE for experiments within the FF regime that was not definite and differed whether it was estimated from the pressure fluctuations or from the local voidage or heat transfer fluctuations. In addition, KE values were almost invariable along the riser over a given height.

3.2. Symbolic dynamics theory

Symbolic dynamics is a methodology that can be employed to enhance certain features of experimental time series of observables in continuous systems. Briefly, the method transforms the time series of an observed variable into a series of symbols, following certain criteria. The degree of discretization can be severe. However, if it is properly done, it can help highlighting features, which may act as indicators of the underlying flow regime, and to monitor the quality of the dynamics of the system from which the experimental time series was obtained (Daw et al., 2003; Godelle and Letellier, 2000; Finney et al., 1998).

There are two procedures that can be used to assign symbols from the measured variables, known as static and dynamic symbolization. In the static symbolization, partitions used to define the symbols are determined from the range of experimental observations. The range can be partitioned, for instance, in equally spaced regions or in order to get equal probability of the defined symbols. After defining the symbols, the ''symbolic words'' or symbol-sequences are computed by establishing a length and assigning an index to the corresponding symbolic word.

From the time series of symbol-sequences, histograms that provide the relative frequency (probability) of appearance of the symbolic words can be calculated. The relative frequency of a certain symbol-sequence provides indications on specific patterns of the time series that can be related to properties of the underlying system. Once the histograms are calculated, statistics can be computed from them to examine particular features of the original time series, or to evaluate significant differences of the underlying system dynamics.

3.2.1. Static symbolization

For the static symbolization, the symbols are defined in this case by considering the region of the column where the tracer is located while crossing a certain height. Again, crossings of the tracer through the mid-height of the test section in the upward direction were considered. To define the partitions, the column section is divided in three regions, so as to get equal probability of occurrences for each one. Then, three symbols with equal probability are defined: values in the column core are assigned a ''0'', values close to the column wall are

assigned a "2" and those in between, a "1". The pair of limiting radius required to have equal probability for each symbol are listed in Table 2.

The crossings are more distributed all over the column cross-section for experiments in the FF regime. Also, except for the experiment at the highest solids flux and gas velocity, those in the DPT regime require a large core to capture one third of the upwards crossings through the testing section mid-height. This is naturally related to the lateral particle segregation of the solids in CFBs and the low solids concentration in the core region for experiments in the DPT regime. Solids holdup radial distributions found in these systems by Gamma CT (Bhusarapu et al., 2006) evidenced large solids radial segregation in both the FF and the DPT regimes. However, the annulus was denser and thinner in the DPT regime and less concentrated and thicker in FF regime. For defining the symbols, we have only computed the upwards crossings; still, in the DPT regime, two thirds of the crossings were concentrated close to the column wall, apparently due to the particle fluctuations while slowly descending or staying for long periods in the annulus region.

After transforming the time series of experimental values into a series of symbols, symbolic words or symbol-sequences are computed by observing successive windows of a given length. We have examined symbol-sequences of length 2–4 and we got similar results. The corresponding decimal conversion has been used as an index of the symbolic words. Having three symbols and symbolic words of length n, the total number of possible symbol-sequences is 3^n.

Fig. 4 shows a comparison of the histograms obtained for experiments at different gas velocities and solids flow rates, for $n = 4$ (81 symbol-sequences). The differences in dynamical behavior between the two explored flow regimes are apparent in the estimated histograms. For experiments in the fast fluidization regime, histograms are more uniform than in the dilute transport flow regime, even though some preeminent symbol-sequences are also observed. Preeminent values in the FF regime correspond to successive crossings in the outer sections of the column, for $r/R > 0.5$. On the contrary, for the DPT regime, symbol-sequences point to successive crossings either close to the column wall or in the column core section.

To quantify the difference between histograms in both flow regimes, the entropies commonly used in the theory of information (Cover and Thomas, 1991) are calculated from the relative frequencies of the symbol-sequences, p_i, as

Shannon entropy, also known as information entropy:

$$H = -\sum_i p_i \log_2(p_i) \tag{1}$$

Renyi order-q entropy ($q = 2, 3, 4, \ldots$), which is a generalization of the information entropy providing different weight to the probabilities. It converges to the Shannon entropy for $q = 1$ (Cover and Thomas, 1991; Rènyi, 1961):

Table 2
Influence of the flow regime on characteristic parameters evaluated from the tracer trajectories with tools from the theory of symbolic dynamics

Riser	u_G (m/s)	G_s (kg/m^2 s)	Flow regime	Radius defining symbol partition		Static symbolization		Dynamic symbolization	
				r_1/R	r_2/R	H (bits/s)	$H^q q = 4$ (bits/s)	H (bits/s)	$H^q q = 4$ (bits/s)
CREL	3.20	26.6	FF	0.62	0.82	6.10	4.93	3.05	2.69
CREL	3.20	30.1	FF	0.59	0.80	6.00	4.52	3.06	2.70
SNL	5.56	145.0	FF	0.51	0.75	6.16	5.30	3.09	2.67
CREL	3.90	33.7	Trans/DPT	0.68	0.69	5.63	3.86	2.83	2.28
SNL	5.49	102.0	Trans/DPT	0.83	0.93	5.29	3.45	2.85	2.28
CREL	4.50	36.8	DPT	0.72	0.97	5.30	4.16	2.84	2.25
SNL	7.71	119.0	DPT	0.56	0.81	5.20	3.12	2.96	2.41

r_1 and r_2 are the radius defining symbol partition for the static symbolization that lead to equal probabilities of the tracer crossing each area at mid-height of the test section. Shannon entropy, H, and Renyi order q entropy, H^q, determined from the histograms of considered symbol-sequences, according to Eqs. (1) and (2) (Cover and Thomas, 1991).

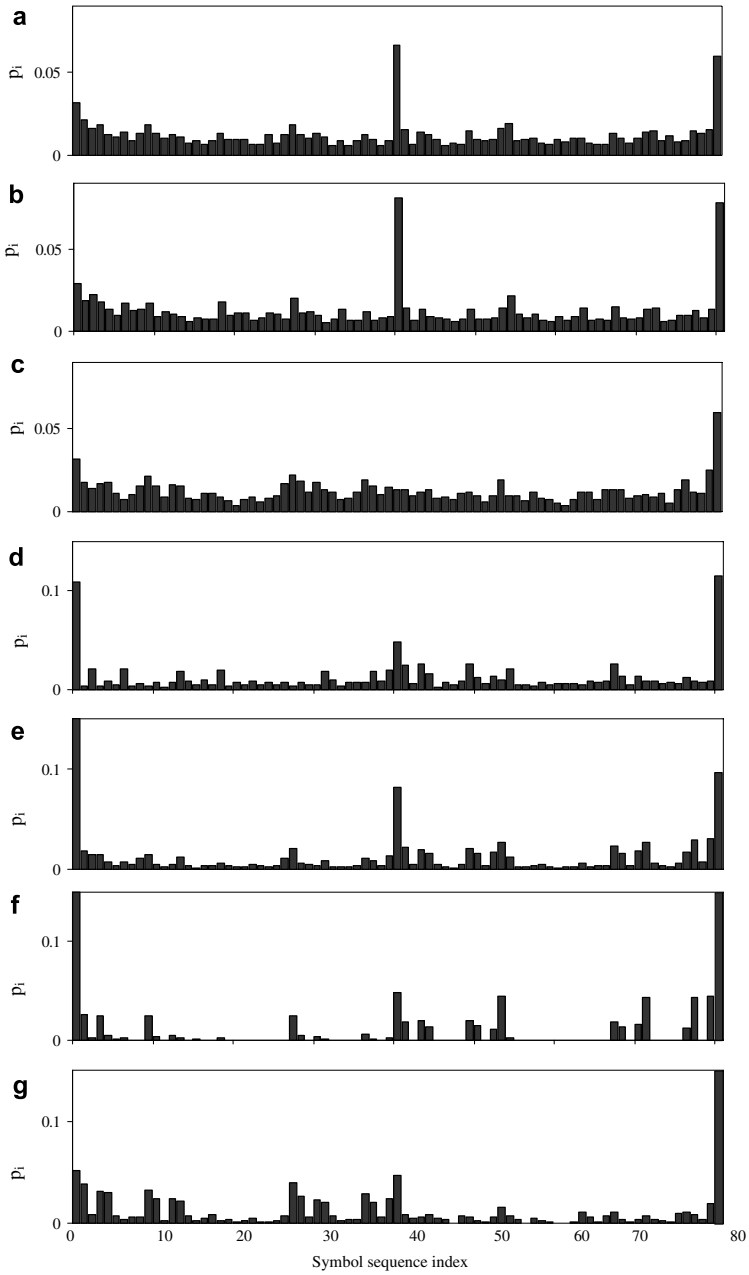

Fig. 4. Histograms of symbol-sequences obtained by a static symbolization strategy, from time series of the tracer trajectories in the riser of the CFBs. (a–c) Fast fluidization regime and (d–g) core-annular dilute phase regime. (a) $u_G = 3.20$ m/s, $G_s = 26.6$ kg/m^2 s – FF; (b) $u_G = 3.20$ m/s, $G_s = 30.1$ kg/m^2 s – FF; (c) $u_G = 5.56$ m/s, $G_s = 145$ kg/m^2 s – FF; (d) $u_G = 3.90$ m/s, $G_s = 33.7$ kg/m^2 s – Trans/DPT; (e) $u_G = 5.49$ m/s, $G_s = 102$ kg/m^2 s – Trans/DPT; (f) $u_G = 4.50$ m/s, $G_s = 36.8$ kg/m^2 s – DPT and (g) $u_G = 7.71$ m/s, $G_s = 119$ kg/m^2 s – DPT.

$$H^q = \frac{1}{1-q}\log_2\left(\sum_i (p_i)^q\right) \tag{2}$$

Estimated values are listed in Table 2. The maximum values that the entropies can attain correspond to uniform histograms; *i.e.*, when the probability is the same for each symbol sequence and equal to the inverse of the number of symbol-sequences considered. The minimum entropies (zero) are calculated when only one

symbol sequence (with unit probability) is found. For the extremes, H and H^q are coincident. The estimated values for the entropies increase as the histogram tends to be more uniform. Hence, as expected from the shape of the histograms and, in agreement with the results obtained from the previous analysis, experiments in the fast fluidization regime present higher values of entropies than those in the dilute transport flow. Again, experiments close to the flow regime transition have histograms similar to those in the DPT regime.

3.2.2. Dynamic symbolization

The dynamic symbolization is generally appropriate to emphasize certain temporal patterns, which are apparent in the analyzed time series. It is the preferred strategy when changes in time are more important than absolute measurements (Daw et al., 2003). One procedure used in dynamic symbolization is to directly assign a symbol to a particular trend of successive measurements (data-mining approach). This approach was used by Cazelles (2004) to compute temporal patterns in animal population time series. Four symbols were defined considering three successive values of the signal (x_{i-1}, x_i, x_{i+1}) according to the following rule:

$x_i \leqslant x_{i-1} \leqslant x_{i+1}$ and $x_i < x_{i+1} \leqslant x_{i-1} \Rightarrow$ a trough, symbol A,
$x_{i-1} < x_i < x_{i+1} \Rightarrow$ an increasing trend, symbol B,
$x_{i-1} < x_{i+1} \leqslant x_i$ and $x_{i+1} < x_{i-1} \leqslant x_i \Rightarrow$ a peak, symbol C,
$x_{i+1} < x_i < x_{i-1} \Rightarrow$ a decreasing trend, symbol D.

The histograms calculated using this dynamic symbolization strategy from the axial coordinate time series of the radioactive tracer measured in the riser of the examined CFBs are shown in Fig. 5. The number of symbol-sequences defined using a length $L = 2$ (*i.e.*, two successive symbols) gives a total number of symbol-sequences of $4^2 = 16$.

As observed, there are two symbol-sequences (marked in black in the histograms), which show significant differences according to the underlying flow regime, irrespective of the facility (CREL or SNL) where the experiments were carried out. The relative frequency of such symbol sequences can be used as a pointer for the flow regime identification. Actually, the whole histogram has a very distinctive pattern for experiments belonging to a certain flow regime, the main feature being the remarkably larger frequencies of symbol-sequences arising from persistent ascending and descending paths of the tracer (BB and DD, respectively) in the FF flow regime. Symbol-sequences associated to fluctuations (AC and CA) have large relative frequency in both regimes, but predominantly in the DPT regime.

The entropies calculated from the histograms are included in Table 2. Once more, the entropies computed from the histograms in the fast fluidization regime are higher than those calculated for the DPT, indicating more complex (uniform) histograms, in agreement with the results calculated from the theory of non-linear dynamics.

It is surprising that the frequencies of fast ascending paths in the DPT regime (symbol-sequence BB) are so scarce compared to the total number of events observed. However, it should be kept in mind that this result corresponds to the whole column, including the dense annulus. To analyze the motion of the tracer within the central region of the column, we have only considered the events while confined to the zone where $r/R < 0.7$ and recalculate the symbol-sequences. This means that we compute a symbol only if there are at least three successive positions of the tracer located within a column core with volume equal to one half of the total column volume. Histograms calculated in this way are shown in Fig. 6. The total number of symbols for each time series is remarkably reduced, but the number is still sufficient enough to get statistically significant results due to the long experimental observation time. Almost all the symbol-sequences disappear, except the ones corresponding to fast ascending trends. This is particularly evident for the DPT regime, where some relative frequencies for the BB symbolic word reach values even larger than 0.9 (almost twenty times more than considering the whole cross-section). In the FF regime, the fast rising paths also increase, they even double with respect to the situation while considering the whole cross-section. However, the difference is quite lower than that of the DPT regime. One feature that comes out as worth to be mentioned is that the fast descending paths (symbolic word DD) are still important in the column core for the FF regime, in sharp contrast to the situation found for the DPT regime, where they are inexistent. These persistent descending paths of the tracer in the column core could be attributed to the existence of descending solids clusters, which entrap the tracer. The

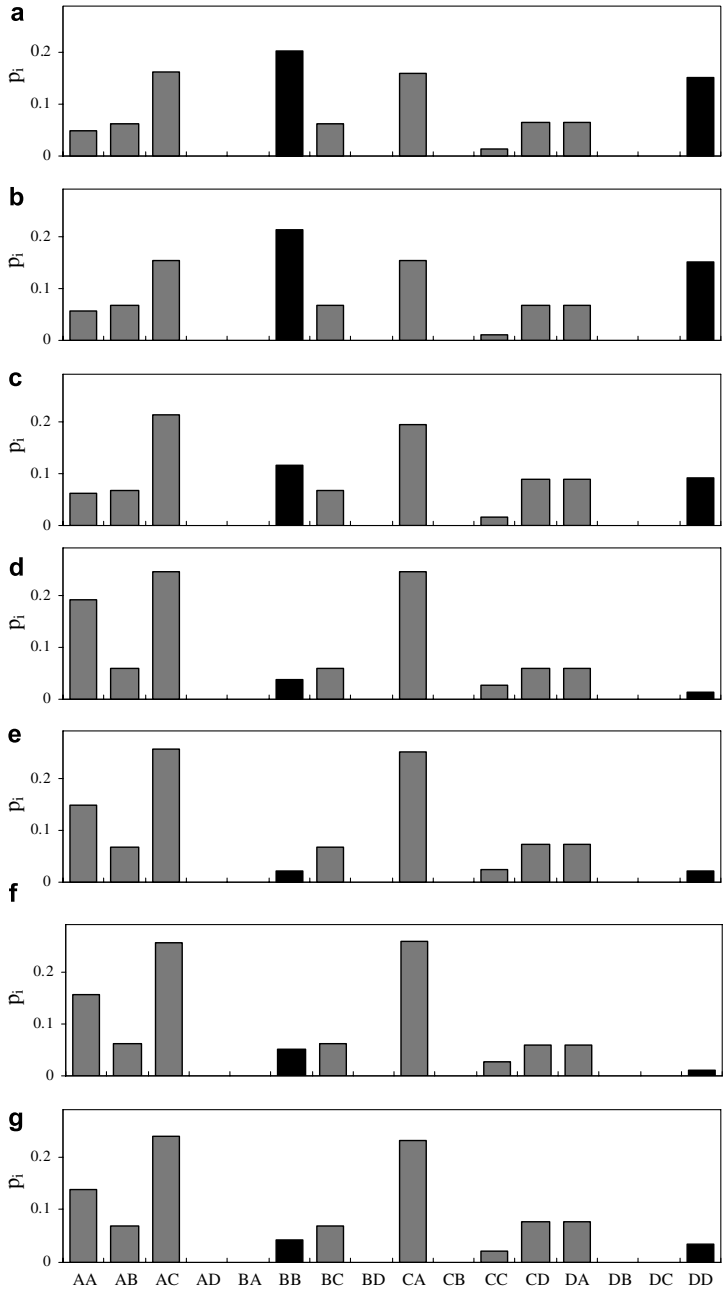

Fig. 5. Histograms of symbol-sequences obtained by a dynamic symbolization strategy from time series of the tracer axial coordinate in the riser of the CFBs. (a–c) Fast fluidization regime and (d–g) core-annular dilute phase regime. (a) $u_G = 3.20$ m/s, $G_s = 26.6$ kg/m^2 s – FF; (b) $u_G = 3.20$ m/s, $G_s = 30.1$ kg/m^2 s – FF; (c) $u_G = 5.56$ m/s, $G_s = 145$ kg/m^2 s – FF; (d) $u_G = 3.90$ m/s, $G_s = 33.7$ kg/m^2 s – Trans/DPT; (e) $u_G = 5.49$ m/s, $G_s = 102$ kg/m^2 s – Trans/DPT; (f) $u_G = 4.50$ m/s, $G_s = 36.8$ kg/m^2 s – DPT and (g) $u_G = 7.71$ m/s, $G_s = 119$ kg/m^2 s – DPT.

existence and flow behavior of solids clusters in CFBs is of particular importance, since they strongly affect reactions outcomes and heat transfer (Huilin et al., 2005; Liu et al., 2005). Mostoufi and Chaouki (2004) have inferred the existence of solids clusters in a gas–solid fluidized bed with high solids flux, from radioactive particle tracking experiments. These authors diagnose the existence of solids clusters from persistent axial motions, at constant velocity, of the radioactive tracer. Following their assumption, previous results indicates

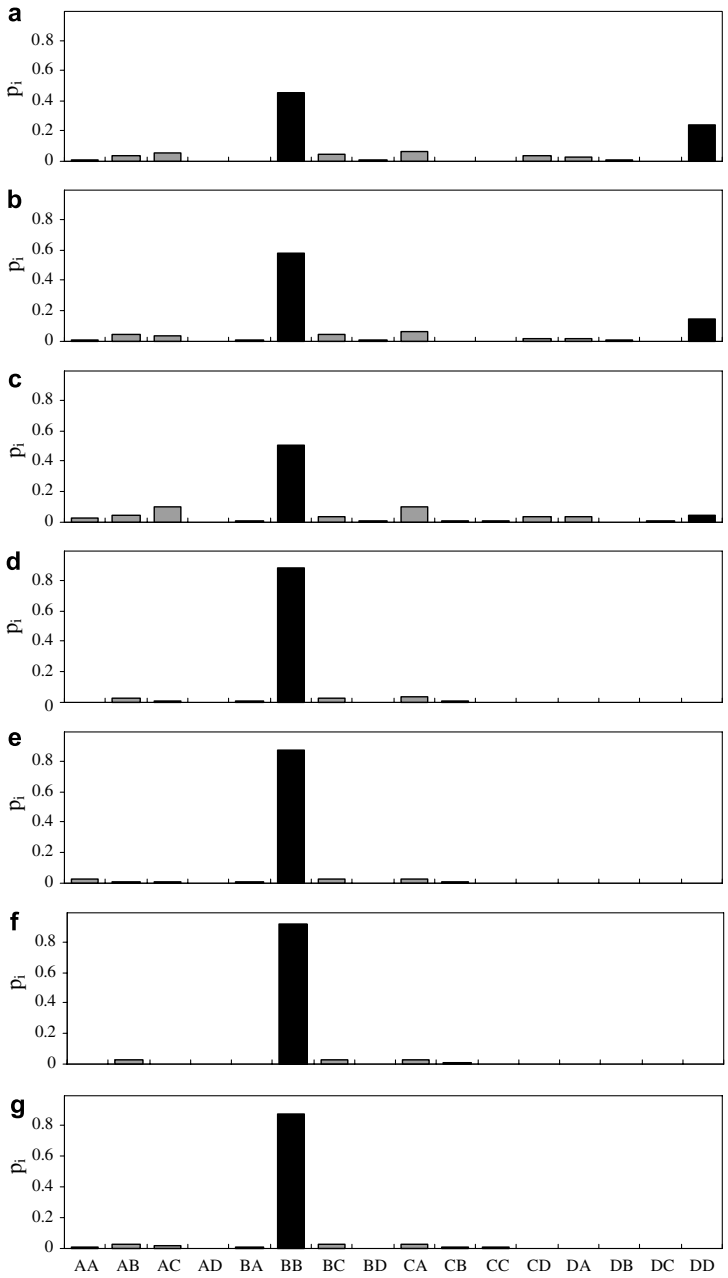

Fig. 6. Histograms of symbol-sequences obtained by a dynamic symbolization strategy from time series of the tracer axial coordinate in the riser of the CFBs, while confined to the column core ($r/R < 0.7$). (a–c) Fast fluidization regime and (d–g) core-annular dilute phase regime. (a) $u_G = 3.20$ m/s, $G_s = 26.6$ kg/m^2 s – FF; (b) $u_G = 3.20$ m/s, $G_s = 30.1$ kg/m^2 s – FF; (c) $u_G = 5.56$ m/s, $G_s = 145$ kg/m^2 s – FF; (d) $u_G = 3.90$ m/s, $G_s = 33.7$ kg/m^2 s – Trans/DPT; (e) $u_G = 5.49$ m/s, $G_s = 102$ kg/m^2 s – Trans/DPT; (f) $u_G = 4.50$ m/s, $G_s = 36.8$ kg/m^2 s – DPT and (g) $u_G = 7.71$ m/s, $G_s = 119$ kg/m^2 s – DPT.

that the existence of descending clusters would not be negligible in the column central region of the riser for the FF regime. This clustering effect has been already interpreted from the velocity PDFs in our earlier work (Bhusarapu et al., 2005, 2006).

By comparing experiments in the FF regime, it is evident that the appearance of persistent dives decreases as the solids mass flux increases (Fig. 6c). Hence, the increase in solids flux would somehow

prevent the solids agglomeration within the column core, pushing upwards the suspended solids in a more definite way. Manyele et al. (2002) have indicated that a decrease in the mean solids concentration results in a higher cluster time fraction in the developed diluted region of a riser in a CFB, particularly for a ratio $r/R < 0.8$. However, they did not observe the existence of downward moving clusters in the riser central region. Liu et al. (2005) also found that an increase in the local time-averaged voidage promotes aggregation of the particles, except for highly diluted systems where the clusters frequency start to decrease. The last would explain the disappearance of descending clusters in the column central region for the DPT regime.

3.3. Data-mining approach

Results shown in Section 3.2 suggest that it is valuable to observe more carefully the persistent descending paths within the column core of the CFBs. Hence, persistent descending paths confined to the column core that last minimum 0.03 s are extracted from the long observation window and examined in detail. Again, a central region with volume equal to one half of the total test section volume is considered; *i.e.*, $r/R < 0.7$. The percentage of time that the tracer remains in the persistent descending paths within the central region of the riser is reported in Table 3. The percentage is calculated with respect to the total time that the tracer stays in the whole testing section. For experiments in dilute phase flow, almost no persistent negative displacements are observed; the percentage of time tends to zero, in coincidence with the results shown in Fig. 6. For experiments close to the transition region, but with dynamical features similar to those in the DPT regime, only very occasional negative excursions are found during the whole observation time. In contrast, in the fast fluidization regime, the percentage climbs over 1% (arising from around 400 paths of more than 0.03 s) for the experiment with the lowest solids mass flux. This value is significantly reduced as the solids mass flux is increased. As previously discussed, descending paths in the central region could be related to aggregation of particles that end up in a cluster that reverses its way. As the solids flux is increased, the probability of collisions and subsequent break of the cluster with the rising solids flow is larger. Hence, the descending trajectories are significantly reduced. Very high gas velocities also prevent aggregation (Manyele et al., 2002), leading to the disappearance of negative trajectories within the core region in the DPT flow regime.

Fig. 7 illustrates a few of the descending paths, typically found in the FF regime at low and high solids mass flux. For the experiment with low solids flux (Fig. 7a), the tracer traverses almost the whole testing section in about 0.12 s, continuously descending and vibrating only slightly in the radial direction. Shown descending trajectories are eccentric from the column center and remain concentrated close to a given position in the x–y projection. In contrast, for high solids mass flux, the axial displacements attained in descending paths generally do not expand the whole testing section. This can be attributed both to a more intense pneumatic

Table 3
Characteristics of solids trajectories within the column core

Riser	u_G (m/s)	G_s (kg/m^2 s)	Flow regime	Time in descending flow in the column core (% of total time)	Times the tracer changes direction (% of total number of occurrences)
CREL	3.20	26.6	FF	1.29	0.83
CREL	3.20	30.1	FF	0.75	0.34
SNL	5.56	145.0	FF	0.08	0.61
CREL	3.90	33.7	Trans/DPT	0.003	0.04
SNL	5.49	102.0	Trans/DPT	0.003	0.06
CREL	4.50	36.8	DPT	0	0.02
SNL	7.71	119.0	DPT	0	0.12

Time % estimated from the number of events fulfilling a given criteria, relative to the total number of occurrences in the defined test section.

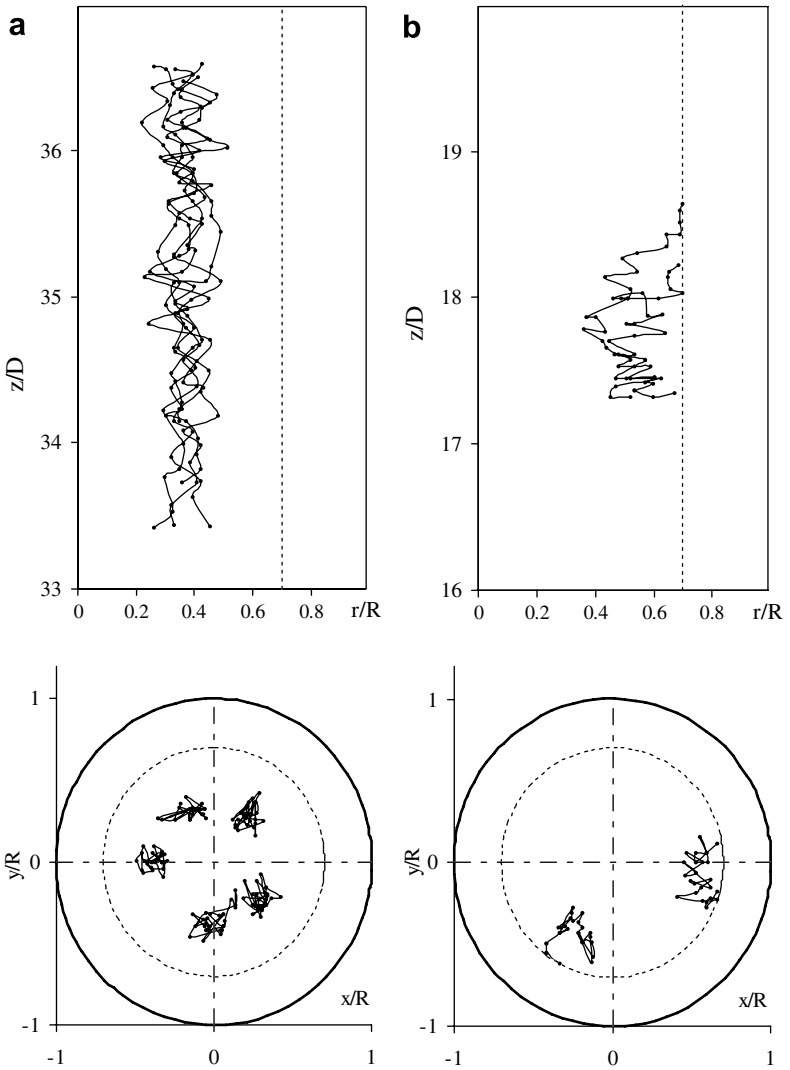

Fig. 7. Characteristics of descending trajectories of the solids tracer within the column central region ($r/R < 0.7$) in the fast fluidization flow regime. (a) $u_G = 3.20$ m/s, $G_s = 26.6$ kg/m^2 s and (b) $u_G = 5.56$ m/s, $G_s = 145$ kg/m^2 s.

effect of the higher gas flow rate and also to the more frequent collisions with other particles moving upwards. The fast descending paths are found closer to the limit of the defined control region than for the low solid mass flux. The x–y projections are broader, arising from a more intense radial vibration in this case, probably due to stronger particle–particle interactions.

Characteristics of the fast descending paths of solid particles, in low mass flux experiments within the FF regime, are evidenced by the probability distributions shown in Fig. 8. The total surface covered by the x–y projections during fast descents, referred to the riser section, is always less than 20% (Fig. 8a). Moreover, the majority of the falls do not expand laterally more than 5% of the riser section, pointing to very sharp drops. These drops cause very fast descending velocities, generally higher than 1 m/s and up to 5 m/s (Fig. 8c) and last no more than 0.3 s (Fig. 8d). Falls are located eccentric to the riser center (Fig. 8b) but quite distributed within the region that goes from 0.2 to 0.6 of the riser radius. Only a few events occur very close to the column center and they are not the fastest ones.

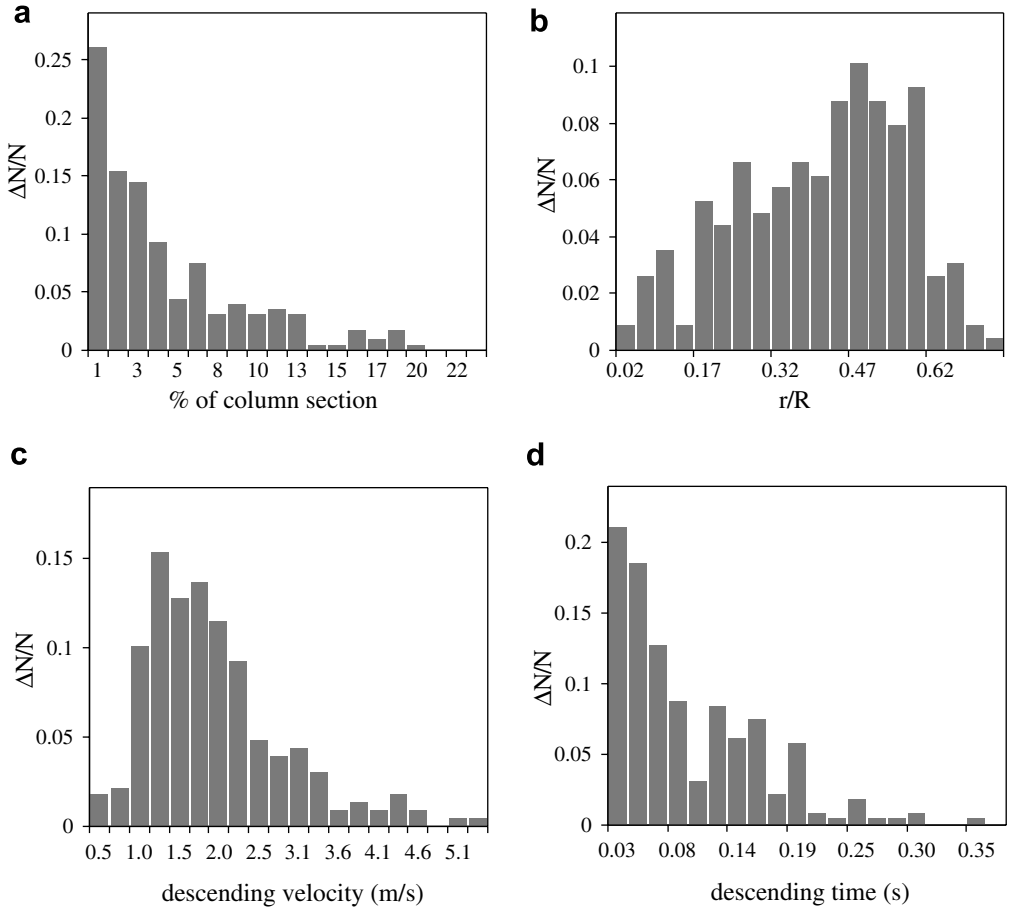

Fig. 8. Characteristics of tracer descending trajectories within the column central region ($r/R < 0.7$) for the low mass flux experiment in the FF regime ($u_G = 3.20$ m/s, $G_s = 26.6$ kg/m^2 s). Probability distributions of: (a) areas of ellipses containing the x–y projections of the tracer position during descending paths, expressed as a percentage of the riser section; (b) radial position of the center of these ellipses; (c) velocities of the tracer during the descending paths and (d) time-span of the fast descending paths.

It was observed that the tracer reverses its direction many times during the tracking period, changing from upwards to downwards and *vice versa*. Direction change could be related to a local recirculation of the solids flow and also to a mass transfer between the core region, where the direction is mainly upwards, and the annulus that predominantly has descending or stagnant solids. In Table 3, the number of times the particle changes direction, with respect to the total number of events in the testing region is reported. Also, the location where this reversal takes place was computed and the radial distribution are shown in Fig. 9 for three experimental conditions. Radial distributions of solid tracer reversal, either from up to down or the opposite, are similar. Events are generally scarce in the column center and more frequent in the outer shell, in coincidence with the solids holdup distribution. However, for the experiment in the FF regime at low solids mass flux, the tracer can reverse its trace almost everywhere, even if more than 50% of the times it changes direction in the outer region of the riser ($r/R > 0.7$). For high solids mass flux, direction changes below $r/R = 0.5$ are negligible both for the FF and the DPT regimes. For the DPT regime, reversals are highly concentrated in the region $0.7 < r/R < 0.9$.

PDFs in Fig. 9 indicate that a simple two zone core-annulus interchange model is insufficient to represent the solids flow pattern in a riser. Further, they also reveal that the interface between the two zones (core and annulus) and the interchange factor are not invariable. Such simplifications in a solids flow model are gross and the PDFs in Fig. 9 provide an indication for modeling the interchange factor.

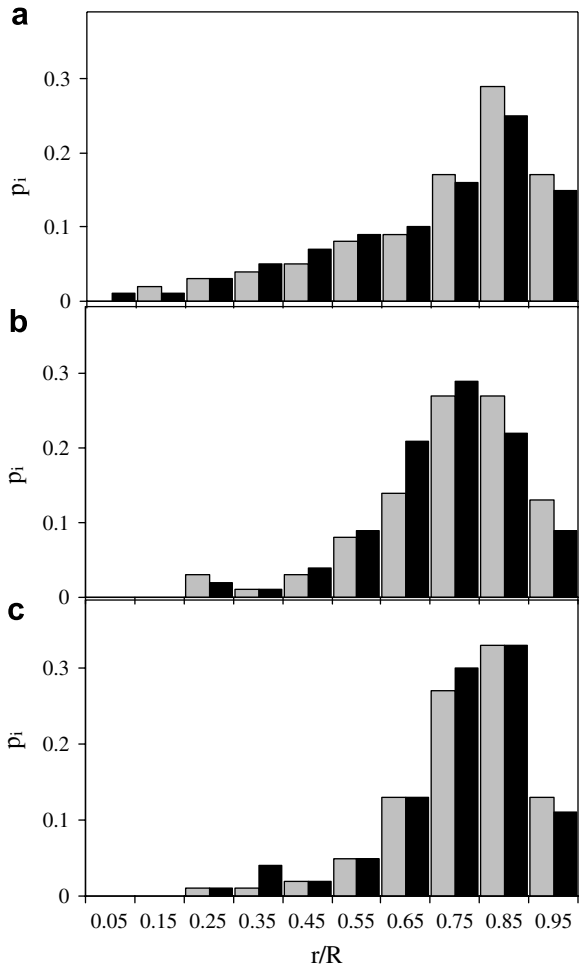

Fig. 9. Radial distribution of locations where the tracer changes direction within the column for: (a) $u_G = 3.20$ m/s, $G_s = 26.6$ kg/m^2 s; (b) $u_G = 5.56$ m/s, $G_s = 145$ kg/m^2 s and (c) $u_G = 7.71$ m/s, $G_s = 119$ kg/m^2 s. Black: upwards to downwards, grey: downwards to upwards.

4. Conclusions

The trajectories of one of the particles traversing a section of the risers of two pilot-scale CFBs have been analyzed with tools from the theory of non-linear dynamics and symbolic dynamics, and from a data-mining approach. The uniqueness of this work is in the application of these data interpretation tools to CARPT data to characterize the fast fluidized and the dilute phase transport regimes.

Maps calculated from successive crossings of the tracer through a given location in the test sections have distinct structure according to the flow regime. They point to a more deterministic and regular motion in the DPT regime than in the FF regime.

Relative frequencies of symbol-sequences derived from the time series of the tracer positions are strongly influenced by the flow regime. Characteristics of these histograms and/or relative frequencies of particular symbol-sequences can be used as pointers of the flow regime.

Both symbolic analysis and a careful examination of the fast descending tracks indicate that there is a downflow motion of solids in the riser core region for the FF regime, particularly at low solids mass flux, while it is totally negligible in the DPT regime. Descending paths in the column core region are very steep and fast, suggesting that they may be due to solids clustering.

Flow reversals of the solids tracer are generally constrained to the outer region of the riser. Direction changes, which could be related to a mass transfer between core and annulus regions, generally peak within the range $0.7 < r/R < 0.9$, and are more concentrated for the DPT regime.

Acknowledgements

The authors thank DOE-OIT for sponsoring the work (Award Number: DE-FC36-01-AL6-7306) as part of MFDRC. Miryan Cassanello acknowledges the Fulbright Foundation for supporting her stay at CREL, and funding from the International Atomic Energy Agency (IAEA-RC12458/R1) and the University of Buenos Aires. Sandia is a multiprogram laboratory operated by Sandia Corporation, a Lockheed Martin Company, for the United States Department of Energy's National Nuclear Security Administration under Contract DE-AC04-94AL8500.

References

Bai, D., Shibuya, E., Masuda, Y., Nakagawa, N., Kato, K., 1996. Flow structure in a fast fluidized bed. Chem. Eng. Sci. 51, 957–966.
Bai, D., Issangya, A.S., Grace, J.R., 1999. Characteristics of gas-fluidized beds in different flow regimes. Ind. Eng. Chem Res. 38, 803–811.
Berruti, F., Chaouki, J., Godfroy, L., Puglsey, T.S., Patience, G.S., 1995. Hydrodynamics of circulating bed risers: a review. Can. J. Chem. Eng. 73, 579–601.
Bhusarapu, S., 2005. Solids flow mapping in gas–solid risers. D.Sc. Thesis, Washington University, St. Louis, MO, USA.
Bhusarapu, S., Al-Dahhan, M., Dudukovic, M.P., Trujillo, S., O'Hern, T.J., 2005. Experimental study of the solids velocity field in gas–solid risers. Ind. Eng. Chem. Res. 44, 9739–9749.
Bhusarapu, S., Al-Dahhan, M., Dudukovic, M.P., 2006. Solids flow mapping in a gas–solid riser: mean holdup and velocity field. Powder Technol. 163, 98–123.
Bhusarapu, S., Fongarland, P., Al-Dahhan, M., Dudukovic, M.P., 2004. Measurement of overall solids mass flux in a gas–solid circulating fluidized bed. Powder Technol. 148, 155–168.
Bi, H.T., Grace, J.R., 1995. Flow regime diagrams for gas–solid fluidization and upward transport. Int. J. Multiphase Flow 21, 1229–1236.
Cassanello, M., Larachi, F., Marie, M.N., Guy, C., Chaouki, J., 1995. Experimental characterization of the solid phase chaotic dynamics in three-phase fluidization. Ind. Eng. Chem Res. 34, 2971–2980.
Cazelles, B., 2004. Symbolic dynamics for identifying similarity between rhythms of ecological time series. Ecol. Lett. 7, 755–763.
Cover, T., Thomas, J.A., 1991. Elements of Information Theory. Wiley-Interscience, New York.
Daw, C.S., Lawkins, W.F., Downing, D.J., Clapp, N.E., 1990. Chaotic characteristics of a complex gas–solids flow. Phys. Rev. A 41, 1179–1181.
Daw, C.S., Finney, C.E.A., Tracy, E.R., 2003. A review of symbolic analysis of experimental data. Rev. Sci. Instrum. 74, 915–932.
Finney, C.E.A., Nguyen, K., Daw, C.S., Halow, J.S., 1998. Symbol-sequence statistics for monitoring fluidization. In: Proceedings of the 1998 International Mechanical Engineering Congress & Exposition (ASME), Anaheim, CA, USA, pp. 405–411.
Godelle, J., Letellier, C., 2000. Symbolic sequence statistical analysis for free liquid jets. Phys. Rev. E 62, 7973–7981.
Grassberger, P., Procaccia, I., 1983a. Measuring strangeness of strange attractors. Physica D 9, 189–208.
Grassberger, P., Procaccia, I., 1983b. Estimation of the Kolmogorov entropy from a chaotic signal. Phys. Rev. A 28, 2591–2593.
Hilborn, R.C., 2000. Chaos and Nonlinear Dynamics. An Introduction for Scientists and Engineers, second ed. Oxford University Press, New York.
Huilin, L., Gidaspow, D., Bouillard, J.X., 1997. Dimension measurements of hydrodynamic attractors in circulating fluidized beds. Powder Technol. 90, 179–185.
Huilin, L., Gidaspow, D., Bouillard, J., 2002. Chaotic behavior of local temperature fluctuations in a laboratory-scale circulating fluidized bed. Powder Technol. 123, 59–68.
Huilin, L., Qiaoqun, S., Yurong, H., Yongli, S., Ding, J., Xiang, L., 2005. Numerical study of particle cluster flow in risers with cluster-based approach. Chem. Eng. Sci. 60, 6757–6767.
Ji, H., Ohara, H., Kuramoto, K., Tsutsumi, A., Yoshida, K., Hirama, T., 2000. Nonlinear dynamics of gas–solid circulating fluidized-bed system. Chem. Eng. Sci. 55, 403–410.
Johnsson, F., Zijerveld, R.C., Schouten, J.C., van den Bleek, C.M., Leckner, B., 2000. Characterization of fluidization regimes by time-series analysis of pressure fluctuations. Int. J. Multiphase Flow 26, 663–715.
Liu, X., Gao, S., Li, J., 2005. Characterizing particle clustering behavior by PDPA measurement for dilute gas–solid flow. Chem. Eng. J. 108, 193–202.
Manyele, S.V., Parssinen, J.H., Zhu, J.X., 2002. Characterizing particle aggregates in a high-density and high-flux CFB riser. Chem. Eng. J. 88, 151–161.
Mostoufi, N., Chaouki, J., 2004. Flow structure of the solids in gas–solid fluidized beds. Chem. Eng. Sci. 59, 4217–4227.
Pallarès, D., Johnsson, F., 2006. A novel technique for particle tracking in cold 2-dimensional fluidized beds – simulating fuel dispersion. Chem. Eng. Sci. 61, 2710–2720.

Rènyi, A., 1961. On measures of information and entropy. In: Proceedings of the 4th Berkeley Symposium on Mathematics, Statistics and Probability, 1960, pp. 547–561.

Schreiber, T., 1999. Interdisciplinary application of nonlinear time series methods. Phys. Rep. 308, 1–64.

Sinclair, J.L., 2000. CFD for multiphase flow: research codes and commercial software. AIChE Symp. Ser. 323, 138–146.

Sprott, J., 2003. Chaos and Time Series Analysis. Oxford University Press, Great Britain.

Takens, F., 2003. Linear versus nonlinear time series analysis – smoothed correlation integrals. Chem. Eng. J. 96, 99–104.

van den Bleek, C.M., Coppens, M.O., Schouten, J.C., 2002. Application of chaos analysis to multiphase reactors. Chem. Eng. Sci. 57, 4763–4778.

Wu, B., Briens, L., Zhu, J.-X., 2006. Multi-scale flow behavior in gas–solids two-phase flow systems. Chem. Eng. J. 117, 187–195.

Zijerveld, R.C., Johnsson, F., Marzocchella, A., Schouten, J.C., van den Bleek, C.M., 1998. Fluidization regimes and transitions from fixed bed to dilute transport flow. Powder Technol. 95, 185–204.